

PassiveVLP: Leveraging Smart Lights for Passive Positioning

WEIZHENG WANG, TU Delft, the Netherlands

QING WANG, KU Leuven, Belgium

JUNWEI ZHANG and MARCO ZUNIGA, TU Delft, the Netherlands

Positioning based on visible light is gaining significant attention. But most existing studies rely on a key requirement: The object of interest needs to carry an optical receiver (camera or photodiode). We remove this requirement and investigate the possibility of achieving accurate positioning in a *passive* manner—that is, without requiring objects to carry any optical receiver. To achieve this goal, we propose PassiveVLP, in which *we exploit the reflective surfaces of objects* and the unique propagation properties of LED luminaires. We present geometric models, a testbed implementation, and empirical evaluations to showcase the opportunities and challenges posed by this new type of passive positioning. Overall, we show that our PassiveVLP can track with high accuracy (a few centimeters) a subset of an object’s trajectory, and it can also identify passively the object’s ID.

CCS Concepts: • Computer systems organization → Embedded systems; • Networks → Cyber-physical networks;

Additional Key Words and Phrases: Visible light positioning (VLP), visible light communication (VLC), passive, reflection of light, system design, implementation, evaluation

ACM Reference format:

Weizheng Wang, Qing Wang, Junwei Zhang, and Marco Zuniga. 2020. PassiveVLP: Leveraging Smart Lights for Passive Positioning. *ACM Trans. Internet Things* 1, 1, Article 3 (February 2020), 24 pages.

<https://doi.org/10.1145/3362123>

1 INTRODUCTION

Thanks to advances in the area of Visible Light Communication (VLC), we now have the ability to piggyback wireless communication on top of LED illumination. This technological breakthrough is creating a new range of exciting applications: positioning/localization [Kuo et al. 2014; Li et al. 2014; Li and Zhou 2018; Philips 2015; Yang et al. 2017; Zhang et al. 2015; Zhang and Zhang 2017], Internet connectivity via luminaires [802.11.bb 2018; PureLiFi 2012], and a new generation of interactive toys [Corbellini 2014], to name a few. Among these applications, positioning is arguably one of the areas that is benefiting the most. This is due to the fact that visible light waves have

This work was supported in part by the Netherlands Organization for Scientific Research (NWO) Top Grant 612.001.854, the Social Urban Data Lab (SUDL), Amsterdam Institute for Advanced Metropolitan Solutions (AMS), the Research Foundation Flanders (FWO) postdoctoral fellowship under grant number 12Y0919N, and the FWO Strategic Basic Research (SBO) project SAMURAI.

Authors’ addresses: W. Wang, J. Zhang, and M. Zuniga, TU Delft, Van Mourik Broekmanweg 6, Delft, 2628 XE, the Netherlands; emails: w.wang-14@tudelft.nl, zhagjunwei@gmail.com, m.a.zunigazamalloa@tudelft.nl; Q. Wang, KU Leuven, Kasteelpark Arenberg 10 - box 2444, Leuven, 3001, Belgium; email: qing.wang@ieee.org.

Permission to make digital or hard copies of all or part of this work for personal or classroom use is granted without fee provided that copies are not made or distributed for profit or commercial advantage and that copies bear this notice and the full citation on the first page. Copyrights for components of this work owned by others than ACM must be honored. Abstracting with credit is permitted. To copy otherwise, or republish, to post on servers or to redistribute to lists, requires prior specific permission and/or a fee. Request permissions from permissions@acm.org.

© 2020 Association for Computing Machinery.

2577-6207/2020/02-ART3 \$15.00

<https://doi.org/10.1145/3362123>

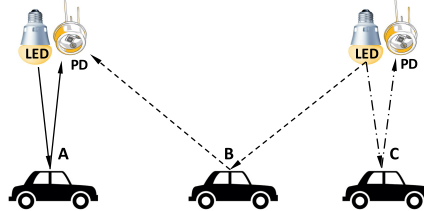


Fig. 1. The concept of passive positioning with smart lights. Three regions A , B , and C can be detected under this simple configuration (PD: photodiode).

propagation properties that are well suited for estimating range: They attenuate in a smooth and rather deterministic manner. For example, when simple trilateration methods are used with radio frequency signals such as Wi-Fi—which are notorious for having severe multipath effects—the positioning accuracy is between 2 m and 6 m [Mok and Retscher 2007]. But the same trilateration methods provide sub-meter accuracy when VLC-enabled luminaires are used as anchor emitting beacons [Li et al. 2014].

Research problem. Current positioning methods based on VLC [Kuo et al. 2014; Li et al. 2014; Li and Zhou 2018; Philips 2015] provide high accuracy but share an important constraint: They require objects to carry photosensors to decode the beacons sent by luminaires. In PassiveVLP, our target is to unleash the constraint of current visible light positioning methods. We remove this constraint and investigate passive visible light positioning—that is, positioning in scenarios where the object of interest does not carry any photosensor. The case we make to investigate *passive* positioning is simple: When objects do not carry photosensors, the only areas that are *constantly* exposed to light are their external surfaces, thus, it is important to *investigate the interaction between VLC luminaires and the reflections coming from these external surfaces to identify cues for positioning*. *Passive* positioning with visible light can be tailored for both static objects and moving objects. The positioning for static objects can exploit the ideas from Li et al. [2015] and Xu et al. [2017]. It requires to attach a retro reflector on the surface of the object. Then the system will pinpoint the object according to the light intensities bounced back from the retro reflector to receivers. The positioning for moving objects is more appealing to us. Considering this type of scenario, we want to understand under what conditions such a positioning system would work and what would the expected accuracy be.

Figure 1 captures the limitations of a naive implementation of passive positioning with visible light. Consider two luminaires that send periodic beacons \mathcal{L}_1 and \mathcal{L}_2 . Each luminaire has a photodiode (PD) attached to it. In general, the PDs co-located with the luminaires may not be able to hear those beacons back due to the low reflectivity of ground surfaces. But if a mobile object with a high reflective surface passes by, the PDs will receive their own (or a neighboring) beacon and, thus, be able to detect the presence of the object. For example, if luminaire \mathcal{L}_1 hears its own beacon, it will infer that an object is in region A , and if it hears a beacon from luminaire \mathcal{L}_2 , it will infer that an object is in region B . But this basic configuration has three drawbacks: *poor coverage*, few positions can be detected (regions A , B , and C , in this case); *coarse-grained accuracy*, the exact location of the object cannot be determined, because we do not know the reflecting angles (shape) of the object; and *there is no identification*, this system can only determine the presence of an object but not its ID—if more than one object is present, the objects cannot be distinguished.

Passive visible light positioning could be applied to scenarios where objects move on established paths in illuminated areas, e.g., mining tunnels or underground trains and vehicular systems. In

those underground scenarios, radio-based solutions face severe multipath effects, rendering most of those approaches inaccurate.

Our contributions. We propose a novel *passive* positioning system to overcome the above described limitations. Our contributions in this new area are listed below:

- (1) *Geometric model for positioning* (Section 2). We develop a geometric model to identify guidelines for the proper design of the transmitters (luminaires), improve the detection coverage, and increase the positioning accuracy. The model gives us insights on how to design the transmitters (luminaires) and on what type of objects can be localized with high accuracy.
- (2) *Passive identification* (Section 3). To identify the objects moving under the luminaires, we embed barcode-like IDs onto the objects' surfaces and propose a novel framework to decode these IDs via passive reflections.
- (3) *Implementation* (Section 4). We design and implement a testbed to evaluate our system. To test short-range scenarios, we modify an open platform. For medium-range scenarios, we develop our own VLC transmitters using standard off-the-shelf LED bulbs.
- (4) *Evaluation* (Section 5). We evaluate our system under three different scenarios with increasing levels of complexity. Our results show that we can pinpoint with cm accuracy a subset of the object's trajectory, and we are able to identify the object's ID in a passive manner.

2 MODEL FOR PASSIVE POSITIONING

To gain a better understanding about the properties and limitations of passive positioning with visible light, we use two models: the Lambertian source, which models the radiation pattern of LED lights; and a geometric model based on the laws of reflection. In the rest of this article, we focus on one-dimensional topologies and assume that (i) *LED luminaires are VLC transceivers* (they can transmit information by modulating their light intensity, and they have a photodiode to receive VLC packets), and (ii) the reflective coefficient of objects is higher than that of the surface where the object is moving on.

2.1 Detecting Objects without Line-of-sight

In VLC, angles play a major role on the received illuminance power. Figure 2 captures this behavior. The wider the irradiation angle ϕ and the wider the incidence angle ψ , the lower the received illuminance. Also, depending on the LED's optical enclosure, the radiation beam can be long and narrow, or broad and short. Formally, these relationships are captured by the well-known Lambertian model H . Denoting P_t as the illuminance power of the LED, the received illuminance power P_r at the photosensor is given by:

$$P_r = P_t \cdot H, \quad (1)$$

where

$$H = \begin{cases} \frac{(m+1)A}{2\pi d^2} \cos^m \phi T(\psi) g(\psi) \cos(\psi), & 0 \leq \psi \leq \Psi_c, \\ 0, & \psi > \Psi_c, \end{cases} \quad (2)$$

where m is the Lambertian order determining the width and length of the beam—a higher m leads to a longer and narrower beam; d is the distance between the LED and the photosensor; A is the detecting area of the photosensor; $T(\psi)$ and $g(\psi)$ are the concentrator and filter gains at the photosensor; and Ψ_c is the field-of-view of the receiver.

The Lambertian model is the pathloss model tailored for line-of-sight communication. It is similar to the Friis pathloss model for radio. Passive positioning relies on reflected beams (no-line-of-sight). To capture the effect of reflections, we modify the above equation based on two properties

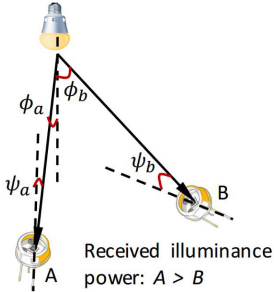


Fig. 2. The Lambertian model.

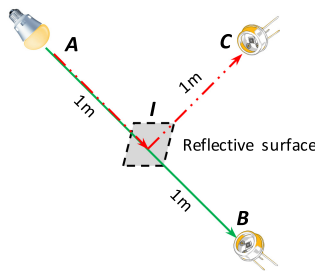


Fig. 3. Capture of reflection effect.

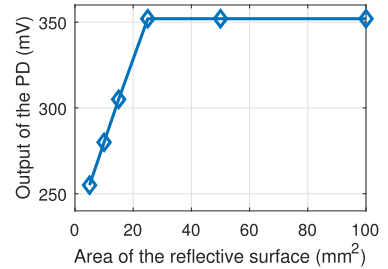


Fig. 4. Impact of the area of the reflective surface (used material is mirror).

Table 1. Measured Combined Coefficient ρ of Different Materials

Material	Mirror	Aluminum	White cardboard
Coefficient ρ	0.89	0.62	0.30

of the reflective surface: its area A_s and its reflective coefficient ρ .

$$HNLOS = Hf(A_s)\rho, \quad (3)$$

where $f(A_s)$ is a linear function of A_s , as explained later. To capture the effect of these two new parameters, we perform the following experiment: First, we set a transmitter and a receiver at a two-meter distance with line-of-sight, as shown in Figure 3, points A and B. Then, we put a reflective surface at point I, one meter away from the LED, and move the receiver to point C (mirror image of point B). In this experiment, we change the area (A_s) and the material (ρ) of the reflective surface. Our results lead to a design guideline for passive positioning.

Guideline 1: Objects with specular reflection and high reflective coefficients are suitable for accurate positioning. Passive positioning with VLC relies on receivers being able to detect reflected messages. The stronger the reflection, the higher the likelihood of detecting an object (better coverage). Upon impinging an object, a reflected light beam loses intensity in two ways: by the way the beam is reflected (shininess) and by how much light is absorbed by the object (reflection). We combine these two effects into a single parameter ρ . Table 1 shows the coefficients we obtained for three different materials. For the particular setup in Figure 3, only two materials, mirror and aluminum, would be localizable in our system, because their reflection coefficients are high enough to allow the decoding of information after reflection.

Guideline 2: The reflective surface of the moving object A_s should be at least the same size as the receiver's area A. Figure 4 depicts the effect of changing the area of the reflective surface. For these experiments, we use mirrors as the reflecting surface. When the area is small, the received illuminance power is low. Beyond a point, however, further increasing the area of the reflective surface does not increase the received illuminance power. This occurs because, with specular reflections, the majority of reflections caused by larger areas do not reach the receiver. Thus, a reflective surface that is smaller than the photosensor's surface affects coverage, because it reduces the likelihood of detecting the object.

2.2 Achieving Full Coverage

The previous subsection indicates that an object only requires a small reflective area to be localized. But this approach only provides limited coverage. In the simplest case, considering N luminaires,

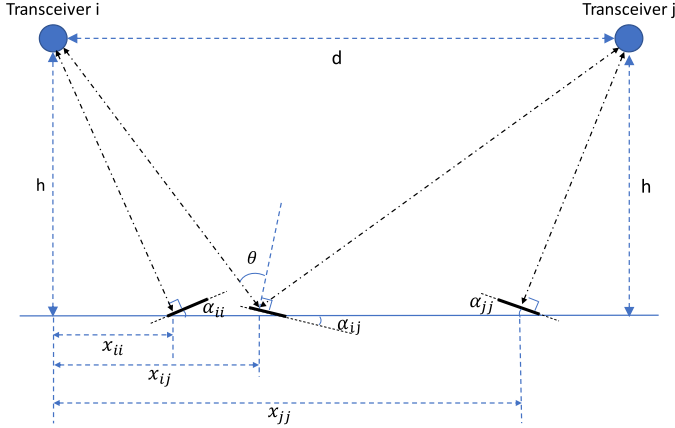


Fig. 5. The illustration of the existences of α_{ij} (Proposition 2.1) as well as α_{ii} and α_{jj} (Proposition 2.2).

we would only be able to identify $2N - 1$ points. The N points under the luminaires and the $N - 1$ intermediate points. However, since the size of the reflective surface can be small, an object can carry an array consisting of many small reflecting surfaces but tilted at different angles. The different angles will reflect beams towards the receiver at different locations, improving coverage. Based on simple geometry, we can make the following propositions based on Figure 5:

PROPOSITION 2.1. *Given two neighboring luminaires i and j , with an inter-distance d and height h from the ground, for any given position x between the lights, there is a tilted angle that will reflect light towards a neighboring transceiver:*

$$\alpha_{ij} = \frac{\arctan\left(\frac{d-x}{h}\right) - \arctan\left(\frac{x}{h}\right)}{2},$$

where clockwise turns denote positive direction of angles.

PROOF. We leverage Figure 5 to help visualize the proof. Letting θ be the incidence angle of light on the object, α_{ij} is given by:

$$\alpha_{ij} = \arctan\left(\frac{d-x}{h}\right) - \theta,$$

and we can see that

$$\theta = \frac{\arctan\left(\frac{d-x}{h}\right) + \arctan\left(\frac{x}{h}\right)}{2}.$$

Hence,

$$\alpha_{ij} = \frac{\arctan\left(\frac{d-x}{h}\right) - \arctan\left(\frac{x}{h}\right)}{2}. \quad \square$$

Based on Proposition 2.1, we can get:

PROPOSITION 2.2. *For a given position x , there always exists a tilted angle that can make the object reflect light back towards the same transceiver:*

$$\alpha_{ii} = -\arctan\left(\frac{x}{h}\right), \quad \alpha_{jj} = \arctan\left(\frac{d-x}{h}\right). \quad (4)$$

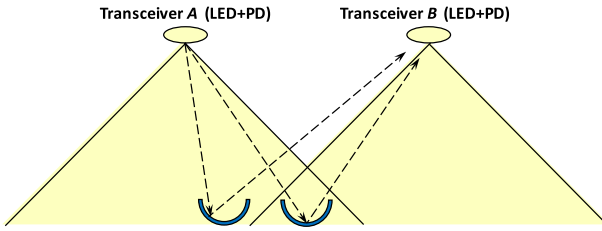


Fig. 6. The problem of unique signature when each transceiver has a single beam. (*The object has many tiny reflective surfaces tilted at different angles—kind of a “retro-reflector”—to improve the coverage.*)

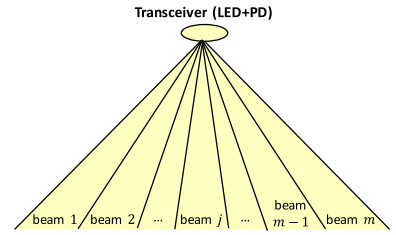


Fig. 7. A transmitter with m beams. (*Here, for simplicity, we use a triangle instead of the Lambertian shape to represent the coverage of an LED.*)

PROOF. We leverage Figure 5 to help visualize the proof. For α_{ii} and α_{jj} , the incidence angle of the light on the object is 0. α_{ii} and α_{jj} are equal to the irradiation angle of the light, which is $\arctan(\frac{x}{h})$ or $\arctan(\frac{d-x}{h})$. Considering the positive direction of angles, we get that

$$\alpha_{ii} = -\arctan\left(\frac{x}{h}\right),$$

and

$$\alpha_{jj} = \arctan\left(\frac{d-x}{h}\right). \quad \square$$

Guideline 3: *A small polyhedral-reflector can be added on top of the object to provide constant coverage.* Consider an object with a reflective coefficient that is too low to reflect a VLC message. Such an object could not be localized in our system. To solve this problem, we can add polyhedral-reflectors to provide better coverage. A polyhedral-reflector can be created to reflect a wide incoming beam (cm^2) into many outgoing narrow beams (mm^2) in different directions. Note that even if an object has a high reflective coefficient, a polyhedral-reflector can still be used to increase coverage, since few objects have surfaces with multiple tilted angles.

2.3 Obtaining Unique Signatures

Until now, our guidelines have focused on the issue of coverage (i.e., increase the number of detected points). But we have not tackled the issue of obtaining a unique fingerprint for each detected point. To highlight this problem, let us use Figure 6. Independently of the location of the object, a neighboring light will always receive the same ID and, thus, it would not be possible to identify the location of an object. For example, in Figure 6, Luminaire B receives the same beacon for the two positions of the convex surface and, thus, it cannot pinpoint the exact location. One way to discern two locations with the same beacon-ID is to use the RSS. But due to the intricate relation among the irradiation and incident angles, the Lambertian order m and the distance traveled d , we observed three problems. First, except for a few points, most RSS values map to multiple locations. Second, the sensitivity of simple photodiodes is not sufficient to distinguish small changes in RSS. Third, under some lighting conditions, the photodiodes can receive the beacons reflected by the ground, which affects the RSS.

Due to the limitations of RSS, we propose to use luminaires with multiple beams, as shown in Figure 7. Instead of having a single wide beam with a low Lambertian order, we propose to use multiple narrow beams with higher Lambertian order. Notice that the overall power does not need to increase, since each narrow beam requires less energy to attain the same range as a wide beam. In our system, each beam emits a unique ID tuple $\langle \mathcal{L}, \mathcal{B} \rangle$, where \mathcal{L} denotes the ID of the luminaire and \mathcal{B} the ID of the beam within that luminaire.

Guideline 4: Luminaires should be designed with multiple beams—the more beams, the better. It is important to highlight that standard off-the-shelf LED lights already consist of multiple internal LED substrates. Many of these LED substrates point to different directions. Designing VLC luminaires for passive positioning would entail adjusting the angles of some of these beams and providing each beam with a unique ID \mathcal{B} .

2.4 Positioning Algorithm

Assuming a set of luminaires and objects following our guidelines, the positioning algorithm works as follows:

- Step 1:** The algorithm requires as inputs: the inter-node distance d , the height of luminaires h , the FoV of the photosensor ω , the number of beams at each luminaire b , a vector μ with the directional angles of the beams, and a vector containing the k tilted angles of the reflector (surface) $\{\alpha_1, \dots, \alpha_k\}$.
- Step 2:** Using Proposition 1, the transceiver calculates the locations \hat{x}_i for all the tilted angles $\alpha_i, i = 1, \dots, k$. At this point, we have k possible locations for the moving object.
- Step 3:** Upon receiving a beacon from a neighboring light, or from itself, the algorithm computes the region covered by that beam: $[x_{\mathcal{L}, \mathcal{B}}^1, x_{\mathcal{L}, \mathcal{B}}^2] = [h \tan(\mu_{\mathcal{L}, \mathcal{B}} - \omega/2), h \tan(\mu_{\mathcal{L}, \mathcal{B}} + \omega/2)]$. At this point, we know the object is under the coverage of beam $< \mathcal{L}, \mathcal{B} >$, but we do not know exactly where.
- Step 4:** The only valid locations \hat{x}_i (Step 2) are those that fall in the range $[x_{\mathcal{L}, \mathcal{B}}^1, x_{\mathcal{L}, \mathcal{B}}^2]$ (Step 3). If only one estimation \hat{x}_i falls in this range, \hat{x}_i is given as the object's location. If multiple estimations fall in the range, the algorithm either returns the average as the location or chooses one of the estimations with higher probability if the direction and velocity of the target can be estimated with prior points.

3 PASSIVE IDENTIFICATION

Positioning an object is not enough. We now introduce how to further *identify* the object *passively* in our system.

Our approach is inspired by a recent work that leverages ambient light for passive communication [Wang et al. 2016], which adopts the patterns of distinctive reflecting surfaces to modulate ambient light. In this article, we use a similar method to label objects with unique IDs attached to objects' surfaces, as illustrated in Figure 8. We refer to this “barcode” as *object-ID*. We use materials with different reflection coefficients to build an object-ID, e.g, aluminum (high) and black paper (low). To decode an object-ID at the PD according to the light it reflects, we have to tackle two challenges:

- *Overlapping signals containing the beam-ID and object-ID.* As presented in Section 2, each transmitter sends modulated light containing its *beam-ID*. At certain positions, this modulated light can be *reflected* by the object's surface to the PD and be used to localize the object. But the *object-ID* also *modulates* the impinging light, albeit at a lower frequency. Thus, the PD will receive an overlapping signal containing both the beam-ID and the object-ID, as illustrated in Figure 9. To identify the object, we need to extract the signal that only contains the object-ID from the overlapping signal.
- *Inter-Symbol Interference (ISI).* At some positions, different parts of the object-ID can reflect concurrently the light coming from two neighboring beams. Therefore, the light modulated by the object-ID may contain interference caused by itself—namely, an ISI effect. As illustrated later in Figure 13 of Section 3.2, the lights of beam-1 and beam-2 are modulated by the third symbol (at point A) and the first symbol (at point B) of the object-ID, respectively.

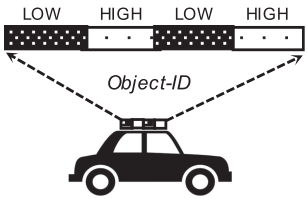


Fig. 8. Attach barcode-like ID to the object's surface.

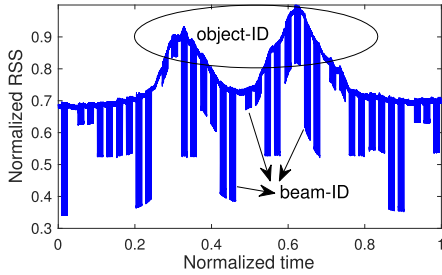


Fig. 9. Illustration of the overlapped signal.

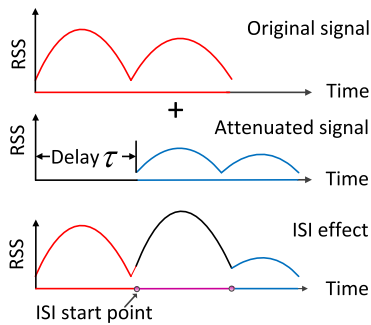


Fig. 10. Illustration of the inter-symbol interference.

This generates ISI at the PD, as shown in Figure 10. Assuming that the object traverses point *A* first, then the signal modulated at point *B* is *actually an attenuated and delayed* version of the original modulated signal at point *A*. In the rest of this article, we refer to these two types of signals as *attenuated signal* and *original signal*, respectively.

3.1 Decoupling of Overlapping Signals

We tackle this problem by proposing a downsampling-based method motivated by the following observations: (*i*) The signal containing the beam-ID is a *high-frequency signal* (created by modulating LEDs at high speed) while the signal containing the object-ID is a *low-frequency signal* (created by the object's movement); (*ii*) When the LED transmits OFF symbols (namely, LED is off), there is a drop in the signal intensity received at the PD, as shown in Figure 9. However, when transmitting ON symbols (namely, LED is on), no drop exists. *In other words, the overlapping signal only occurs when OFF symbols are transmitted. Thus, we just need to remove the OFF symbols from the overlapped signals.* The proposed downsampling method works as follows:

- (1) Guarantee that there are no continuous OFF symbols in the modulated data at the LEDs. This is a necessary requirement to remove the OFF symbols in our method. To achieve this, we use the following modulation at transceivers: Use a symbol sequence of OFF-ON to denote a bit 0, and symbol sequence of OFF-ON-ON to denote a bit 1. This modulation is depicted in Figure 11(a);
- (2) Set the downsampling interval slightly wider than the duration of an OFF symbol. By doing this, we guarantee that each OFF symbol is sampled at most once, as depicted in Figure 11(b);

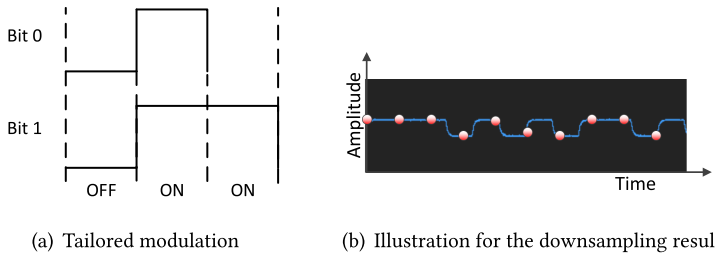


Fig. 11. Proposed downsampling method to decouple overlapping signals.

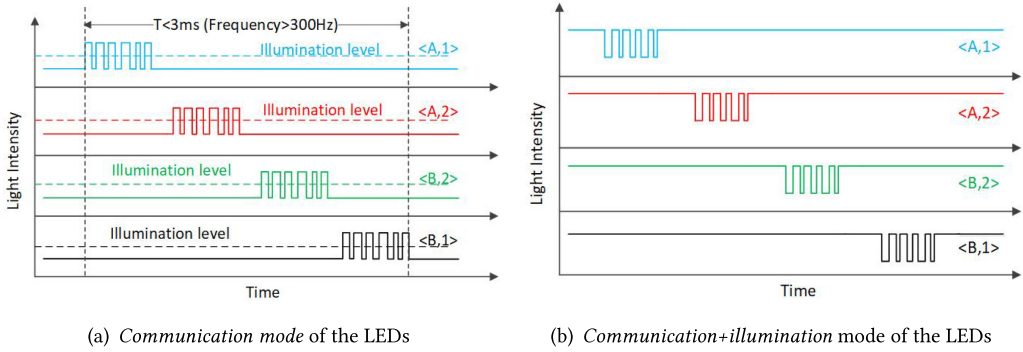


Fig. 12. Operation modes of the LEDs under different ambient light conditions.

- (3) Compare each two adjacent samples: If the difference of two adjacent samples is higher than a threshold (i.e., an abrupt drop occurs in the RSS), then we discard the sample that has a lower value (i.e., remove the OFF symbol).

3.2 Remove the Inter-symbol Interference

As we know, smart lighting has become an effective way to reduce the high energy footprint on artificial lighting. Smart lighting systems adjust the illuminance of artificial lights (normally, LED lights) based on the contribution of ambient natural sunlight in our environment. They are expected to maintain a constant illumination within the area of interest, improving the energy-saving and user comfort [Wu et al. 2017]. Taking this practical requirement into consideration, the ISI problem described at the beginning of Section 3 can be addressed by different methods according to the requirement on artificial illumination from LEDs. In this article, operation modes of the LEDs are divided into two types:

- *Communication mode.* When the ambient light is enough to provide illumination, there will be no demand on artificial LED illumination. Therefore, an LED only needs to be turned on when it is scheduled to send its beacon; otherwise, the LED is turned off. This is depicted in Figure 12(a). When only one LED is turned on at a given time slot, there would not be multiple LED lights added together to form the ISI effect. Therefore, the ISI problem is avoided.
- *Communication+illumination mode.* This mode is enabled when the ambient light is weak. Under this mode, multiple LEDs should be turned on to satisfy the required illumination level. Among these LEDs, one of them is scheduled to transmit its beacon at a given time slot, while the other LEDs are simply turned on to illuminate the surrounding environment,

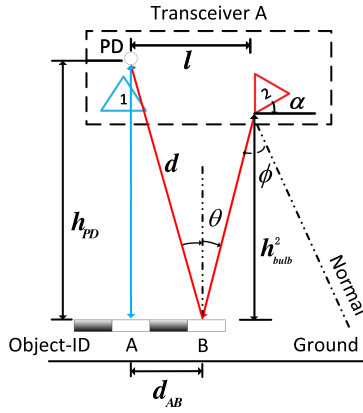


Fig. 13. Illustration of the geometric model used to remove the ISI.

as depicted in Figure 12(b). As we presented at the beginning of Section 3, this is the main reason why we have multiple signals overlapped with each other to bring the ISI effect.

Under the *communication mode* of LEDs, the ISI problem can be avoided easily. However, in reality, the *communication+illumination mode* of LEDs is more common and also more challenging. Therefore, in the rest of this subsection, we will present our general solution to remove the ISI effect considering the *communication+illumination mode* of LEDs.

To eliminate the ISI effect, we propose a method to remove the attenuated signal from the original one. To do this, we need the following information: (1) *delay* of the attenuated signal with respect to the original signal; and (2) *intensity* of the attenuated signal. Next, we present how to obtain this information and how to extract and decode the original signal after that.

- **Obtaining the delay of the attenuated signal.** Consider the scenario in Figure 13. As presented earlier in this section, the ISI starts when the object reaches point B. At this position, a symbol (e.g., the i th symbol) of the object-ID will generate interference by modulating the light emitted by beam-2. Note that this modulated light contains the ID of beam-2 and this beam-ID can be decoded by the PD for localization. Moreover, when reaching point A, this i th symbol has modulated the light emitted by beam-1, and this modulated light carrying the ID of beam-1 has been decoded by the PD as well.

Let t_0 and $t_0 + \tau$ be the time when *for the first time* the PD decodes the IDs of beam-1 and beam-2, respectively. Since the transceiver can modulate light at a very high speed (i.e., it can transmit the frames that contain beam-IDs very frequently), we can assume that t_0 and $t_0 + \tau$ are the time when the object reaches point A and point B, respectively.

Therefore, the difference between t_0 and $t_0 + \tau$ —namely, τ —is the *delay of the attenuated signal*. Note that t_0 and $t_0 + \tau$ can be obtained easily in practice. Besides, at some positions (as will be presented in Section 5.3), τ can be a *negative value*, meaning that the attenuated signal starts *earlier* than the original signal.

- **Obtaining the intensity of the attenuated signal.** To derive this, we still use Figure 13 as an illustration. Let h_{PD} and h_{bulb}^2 denote the heights of the PD and bulb 2, respectively, and let l be the horizontal distance between them. From the geometric model in Figure 13, we can derive the distance d_{AB}

$$d_{AB} = l \cdot \frac{h_{PD}}{h_{PD} + h_{bulb}^2}. \quad (5)$$

Let θ and ϕ be the reflection angle at point B and irradiance angle of bulb 2, respectively. We have $\theta = \arctan \frac{d_{AB}}{h_{PD}}$ and $\phi = \alpha + \theta$. Based on Equation (1), we can obtain the intensity of the attenuated signal modulated by the object-ID at point B :

$$P_{\text{att}}^B = \frac{\rho P_t (m+1) \cos^m(\phi)}{2\pi d^4} T(\theta) g(\theta) \cos(\theta). \quad (6)$$

Similarly, the intensity of the original signal modulated by the object-ID at point A can be expressed as follows:

$$P_{\text{orig}}^A = \frac{\rho P_t (m+1) \cos^m(0)}{2\pi h_{\text{PD}}^4} T(0) g(0) \cos(0). \quad (7)$$

In our model, we can assume that $h_{\text{PD}} \approx h_{\text{bulb}}^2 \gg l$. Then, we have the approximation: $h_{\text{PD}} \approx d$. Besides, there is no optical filter or concentrator in our system. Thus, $T(\cdot)$ and $g(\cdot)$ are constant in our model. Let η denote the *attenuation ratio*, defined as the ratio between the intensity of the attenuated signal and that of the original signal, then we have

$$\eta = \frac{P_{\text{att}}^B}{P_{\text{orig}}^A} = \cos^m(\phi) \cos(\theta). \quad (8)$$

- **Extract and decode the original signal.** To achieve this, from now on, we consider the continuous version of the signals. Following convention, we use $f(t)$ to denote a continuous signal. Let $f_{\text{orig}}(t)$ and $f_{\text{att}}(t)$ be the continuous original signal and the continuous attenuated signal, respectively. We have

$$f_{\text{att}}(t) = \eta f_{\text{orig}}(t - \tau). \quad (9)$$

Let $f_{\text{sum}}(t)$ be the aggregated signal received at the PD, then

$$f_{\text{orig}}(t) = f_{\text{sum}}(t) - f_{\text{att}}(t) = f_{\text{sum}}(t) - \eta f_{\text{orig}}(t - \tau). \quad (10)$$

As presented in Section 3.2, we can denote t_0 as the time when the object-ID reaches point A and $t_0 + \tau$ as the time when the object-ID reaches point B where the ISI appears. Since there is no ISI during the time slot $[t_0, t_0 + \tau]$, we have

$$f_{\text{orig}}(t) = f_{\text{sum}}(t), \quad \forall t \in [t_0, t_0 + \tau]. \quad (11)$$

Based on Equation (10) and Equation (11), we can now obtain the original signal $f_{\text{orig}}(t)$ (without the ISI effect). To decode it, we use a simple threshold-based decoding method (omitted due to its simplicity, limited novelty, and the page limitation).

3.3 Object-ID Design

As mentioned at the beginning of Section 3, we use materials with different reflection coefficients to build an object-ID, e.g., aluminum (of high reflection) and black paper (of low reflection). An object-ID consists of two parts: *object-ID-preamble* and *object-ID-value*. In these two parts, we use materials with both high reflection coefficient (referred to as “HIGH” in the rest of this article) and low reflection coefficient (referred to as “LOW” in the rest of this article) to embed the information. The structure of our designed object-ID is given in Figure 14. The PD’s captured signal of the designed object-ID is illustrated in Figure 15. The *object-ID-preamble* plays an important role in decoding the object-ID at the PD. Therefore, we first present our key considerations when designing the preamble.

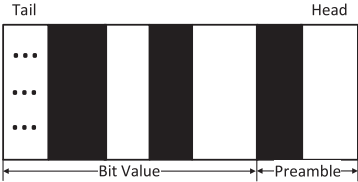


Fig. 14. The structure of our object-ID.

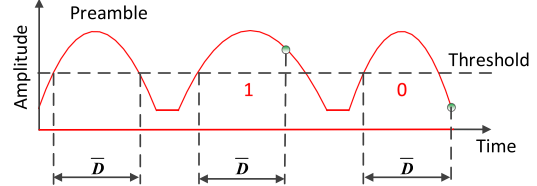


Fig. 15. Illustration of the PD's captured object-ID signal.

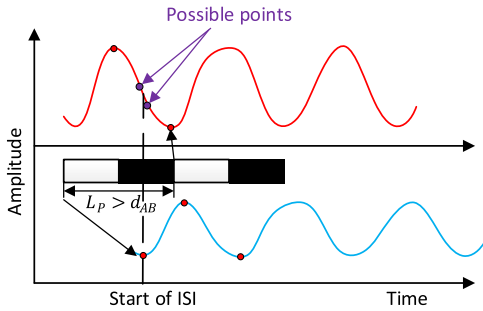


Fig. 16. Illustration of the starting point of the ISI effect.

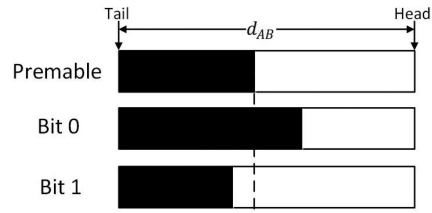


Fig. 17. Bit design in PassiveVLP.

3.3.1 Object-ID-preamble Design. The preamble can be used to obtain the threshold, which is key to decode the following ID part of the object-ID. Besides, it can help estimate the speed of objects. Remember that we have ISI effect when multiple LEDs operate at the *communication+illumination* mode. Although we can remove the ISI effect with the mechanism introduced in Section 3.2, it is better if we can design an *ISI-free object-ID-preamble*. Denote the length of object-ID-preamble as L_p . An improper L_p will bring ISI effect as well as make it difficult to locate the right ISI starting point in the signal. For instance, as illustrated in Figure 16, if L_p is longer than d_{AB} (cf. Figure 13), then the ISI effect occurs and it is not easy to calculate the ISI starting point, which is crucial for the mechanism we propose in Section 3.2.

To avoid the above problem, we design the object-ID-preamble length L_p to be equal to or smaller than d_{AB} . This means that, as illustrated in Figure 16, the attenuated signal starts from the second valley in the original signal (when $L_p = d_{AB}$), or after the second valley (when $L_p < d_{AB}$). In this work, we set $L_p = d_{AB}$. By doing this, we not only achieve an ISI-free preamble for the object-ID, but also know that the ISI starts from the second valley of the original signal. Note that when L_p is too short, it is not easy for the PD to detect the preamble. In passiveVLP, the appearance duration of the Object-ID-preamble at the PD should be much longer than the time needed to transmit a beacon for the PD to correctly decode the beacons. This can be seen clearly from Figure 9, where the duration of object-ID is much longer than that of a beam-ID.

In the preamble, we use one HIGH and one LOW, starting from HIGH, i.e., the preamble has the pattern of HIGH-LOW. The total length of the HIGH and the LOW in the preamble equals to L_p . This design of the preamble is shown in Figure 17. In reality, it is possible that the distance between the object-ID and the ceiling PD varies (e.g., the ceiling is not flat in the underground scenario). Therefore, L_p could not always be the same as d_{AB} . In this case, the second valley in the combining signal will no longer be the ISI starting point. Therefore, we need to find the minimum length of LOW to make the second valley as long as possible to form a flat area. Then, the beginning of the rising trend will become the ISI starting point.

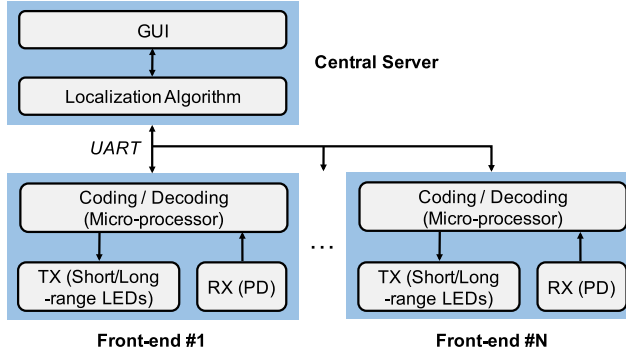


Fig. 18. The function blocks of our PassiveVLP testbed.

3.3.2 Object-ID-value Design. Following the used pattern in the preamble, in the object-ID-value part, we also use the pattern HIGH-LOW to denote each bit of the object ID. For example, if there are four bits to denote the value of the object ID, then we will have four groups of HIGH-LOW in the object-ID-value part. To distinguish between a bit 1 and a bit 0, we use different durations for the HIGH and LOW in the corresponding group of HIGH-LOW, as illustrated in Figure 17.

4 TESTBED

A solid evaluation of passive positioning with VLC requires designing a system where multiple parameters can be adjusted. Below, we describe how we use our design guidelines to build a comprehensive evaluation testbed.

4.1 Luminaire Design

We design our luminaires based on the Shine platform [Klaver and Zuniga 2015]. Shine was originally designed for omni-directional multi-hop communication with visible light. Each Shine node is equipped with 20 LEDs (HLMP-CM1A-450DD, FoV is 18°) and four PDs (SFH203P, FoV is 90°). The micro-controller is an Atmega 328P, which is low-cost but powerful. Shine also provides serial communication capability to interface with a PC/laptop. We extend it largely in both the hardware and software to build our testbed in three ways. First, we improve its reception capabilities, a front-end we refer to as *Shine+*. Second, we add more powerful LEDs to build another front-end referred to as *Shine++*. Third, we modify its software. The block diagram of our new testbed is given in Figure 18. Next, we present the design details of both front-ends.

4.1.1 A Short-range Luminaire with Multiple-beams—*Shine+*. Shine has multiple narrow beams, which follows *Guideline 3*, but it is designed for line-of-sight communication. Since we rely on *non-line-of-sight reflections*, we must improve Shine's reception capabilities. To achieve this goal, we implement two changes. First, we change the PD from SFH203P to SFH206K, which extends the communication range by 165%. Second, we add a low-pass filter to improve the signal-to-noise ratio.

4.1.2 A Medium-range Luminaire with Less-beams—*Shine++*. To evaluate our sensing approach with longer ranges in realistic scenarios, we build a new front-end with commercial LED bulbs, dubbed *Shine++*. We choose the IKEA Ledare LED with a viewing angle of 36° as the transmitters. We use three LED bulbs: one placed in the middle and the other two on the sides with adjustable inclination angles, as shown in Figure 19(a). Each LED consumes 3.5 W; thus, we design a new LED driver circuit to provide higher power, as presented in Figure 19(b).

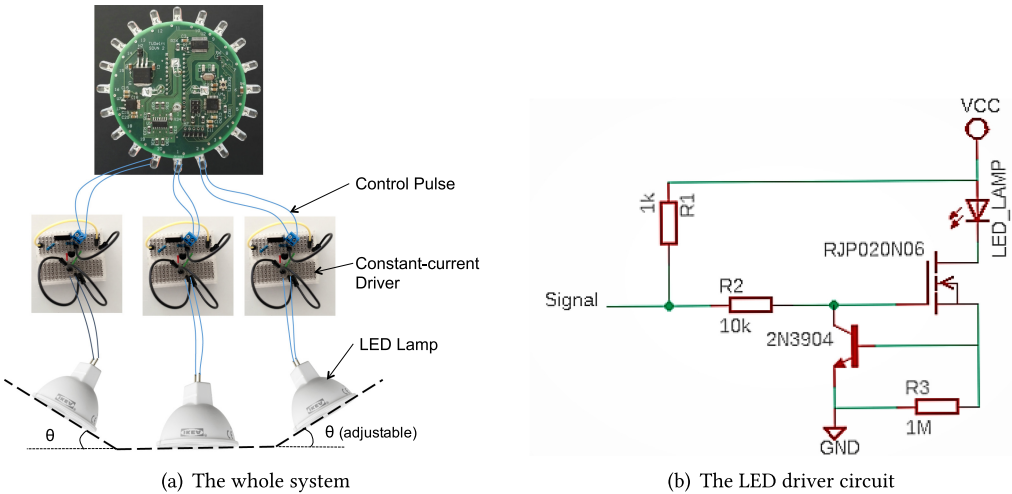


Fig. 19. Our testbed with the front-end Shine++.

4.1.3 Software. Our software implements the data transmission and reception, the access control for the shared visible light medium, and the positioning and object identification algorithms. In our application, we need accurate timing to schedule the modulation of light beams. We connect all the nodes to a central server (PC/laptop), where we run a Time Division Multiple Access (TDMA) scheme. This scheme turns *on* all LEDs, but modulates only one *beam* at a time. Adaptive decoding thresholds are implemented in our system to eliminate interference from external light sources, including neighboring LEDs that are *on* but not modulated. The MAC schedules the LEDs “remotely” through the interface with the micro-controllers. Similarly, the data received from the PDs are decoded at the micro-controllers and sent through the UART to the central server. Upon receiving these frames, the server runs the *positioning algorithm* (cf. Section 2.4) and calculates on-the-fly the current position of the mobile object. The outcome of the algorithm is demonstrated in a simple GUI (omitted due to the space limitation).

4.2 Object Design

For passive positioning with VLC, the external surface of the objects plays a key role. Three out of the four guidelines in Section 2 pertain to the object’s surface. In this subsection, we describe the surfaces we use for our evaluation and the reasoning behind selecting them.

4.2.1 A Perfect Reflector. As stated by our guidelines, the ideal surface would use materials with very high reflective coefficients and specular reflection to enable non-line-of-sight communication, and would consist of small reflecting areas (Guideline 1) tilted at different angles (Guideline 2) to increase coverage. We use thin strips of flat mirrors to satisfy these three guidelines. Figure 20 presents a side view of the reflecting object, which consists of five mirrors with inclined angles of -18° , -9° , 0° , 9° , and 18° , respectively. All the mirrors have the same width of 5 mm.

4.2.2 A Standard Reflector. To evaluate the performance of passive positioning with more standard objects, we use a customized toy car. Such an object relaxes the requirements of our first three guidelines. The material is metal, whose reflective coefficient is not as good as mirrors. Second, the surfaces are big (relaxes Guideline 1). Third, it has few tilted angles (relaxes Guideline 2). For our object, we consider three parts of a car: the front windshield, the roof, and the back windshield. After a thorough investigation of different cars’ shapes, we decided to customize a toy car with

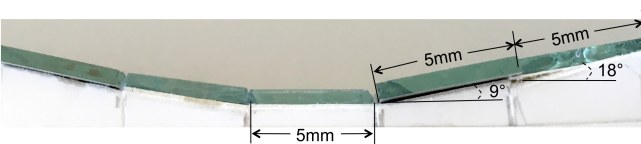


Fig. 20. Side view of the object with *perfect* reflective coefficient.



Fig. 21. Customized toy car (standard reflector, 28cm x 11cm x 7cm).



Fig. 22. The object-ID (preamble + ID value “0”) that is attached to all three parts of the object.

inclined angles of -30° , 0° , and 25° . The final customized car is shown in Figure 21. Note that we are aware of the fact that different parts of a real car have different reflection coefficients, but we only use one type of material for a single toy car in this work for simplicity. We build two different toy cars: one with aluminum and the other one with mirrors.

4.2.3 Design of Object-ID. We label the objects in our system with unique IDs consisting of certain patterns. The ID pattern has been presented in Figure 17. An object-ID consisting of the preamble and a bit “0” is shown in Figure 22 where it is attached to the three faces of the customized toy car.

5 EVALUATION

In this section, we evaluate our methods under increasingly complex test cases. First, we present the evaluation on positioning, followed by the evaluation on identification. Note that our passive positioning and identification methods can work at the same time, as described in Section 5.3.

5.1 Positioning: Ideal Case

For the ideal case, we use the best possible setup: the front-end with many beams (Shine+) together with the perfect reflector. The experiment setup is shown in Figure 23. We deploy two nodes (denoted as A and B) at an inter-node distance of 20 cm and at a height of 15 cm from a desktop. The light intensity measured at the desktop is about 450 lux under the nodes (cf. positions R2 and R10 in Figure 24). Shine+ can achieve reliable VLC at a distance of up to 50 cm. By deploying the two nodes as described above, we can assure that the distance travelled by the reflected signals is shorter than the maximal communication distance (i.e., 50 cm). It is also important to highlight that the angles of the perfect reflector are designed based on Propositions 1 and 2 to guarantee that every beam has at least one angle that will reflect the light to a neighboring node or to itself. If these angles are not selected carefully, the system may end up having beams without reflections, and thus, no positioning could be performed inside the area covered by these beams. Different inter-node distances or heights will lead to different tilted angles.

Results. The evaluation results are shown in Figure 24. The red dots represent the ground truth. The experiments were repeated 10 times, and we did not observe any major variance, which is

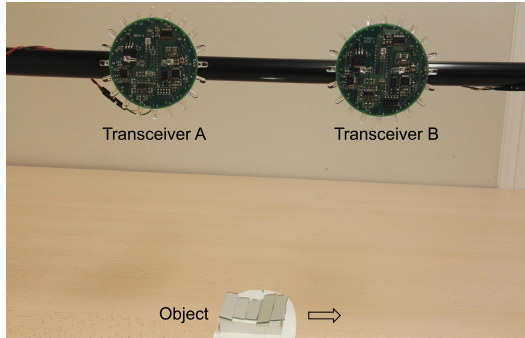


Fig. 23. Experiment setup in the ideal case (height=15 cm, inter-node distance=20 cm).

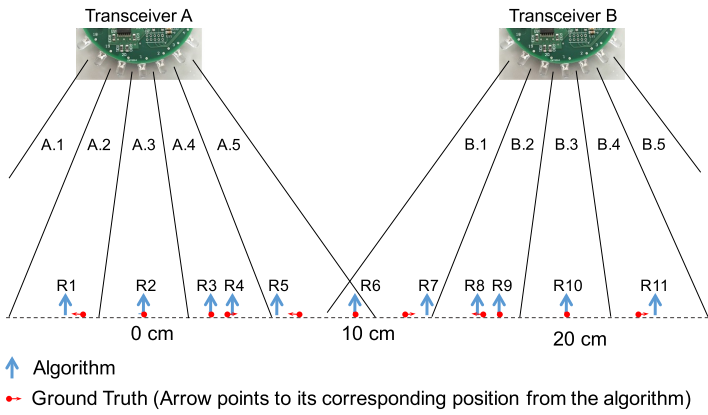


Fig. 24. Evaluation results in the ideal case.

Table 2. Details of the Localized Positions from our Algorithm in Ideal Case (Number: the Detected Locations; TX: Transmitter; RX: Receiver)

Position	R1	R2	R3	R4	R5	R6	R7	R8	R9	R10	R11
Reflection angle	-9°	0°	9°	-18°	18°	0°	-18°	18°	-9°	0°	9°
TX	A.2	A.3	A.4	A.4	A.5	A.5	B.1	B.2	B.2	B.3	B.4
RX	A	A	A	B	B	B	A	A	B	B	B
Calculated position	-4.7	0	4.7	3.3	6.7	10	13.3	16.7	15.3	20	24.7
Measured position	-3.4	0	3.4	4.5	7.9	10	12.1	15.9	16.1	20	23.4

expected due to the rather deterministic propagation properties of light waves and the nearly specular reflection of mirrors. We can observe that the results from our algorithm match well the ground truth. Nearly half of the locations are localized with almost perfect accuracy, while the other locations are detected with errors up to 1.3 cm.

The details on how these locations are detected are given in Table 2. Now let us give some more insights on how our algorithm (cf. Section 2.4) leads to these results. The object moves from left to right. The algorithm has all the inputs required in Step 1. The first detected point $R1$ is a self reflection, i.e., transceiver A receives the reflection of beam $A.2$. The server calculates all the ground truth locations that the set of self-reflecting angles $\{\alpha_1, \dots, \alpha_k\}$ can have (Step 2). Then it

calculates the valid region for this beam $A.2$ (Step 3). The algorithm detects that only one point falls in the valid region and, hence, reports that point as the estimated location. The true location is ≈ 1 cm to the right. The next two estimated locations, $R2$ and $R3$, are also self-reflections. The fourth estimated location, $R4$, is due to the communication between transceivers A and B (inter-node reflection). Notice that in this case, two locations are within the valid region of beam $A.4$: $R3$ and $R4$. But the fact that $R3$ is a self reflection while $R4$ is not helps with distinguishing them. Note that $R4$ does not need to be under the coverage of transceiver B to achieve inter-node reflection. This is because the photodiodes used in our experiments have a wide field of view (90°). A more challenging case occurs with the next two locations ($R5$, $R6$). These two locations are within the valid region of beam $A.5$, and both are the result of inter-node reflection. As stated in Step 4 of our algorithm, we can either average them out at the cost of increasing the error or exploit speed and direction information from prior data to select the most likely location. We implement a very simple mechanism to exploit direction information. Every time we detect a new point, we set it as the origin; prior data are given negative values based on their distance to this last point, and new data are given positive values. If two or more positive points are estimated as locations, we select the closest one (point $R5$ in this case). The remainder half of the path is symmetrical to the first half and, thus, the estimation is similar to what has just been described. We do not have any location estimations for beams $A.1$ and $B.5$, because there are no self-reflecting angles for these regions. If transceiver A would have a neighbor to its left, then beam $A.1$ would have two potential locations (similar to $R6$ and $R7$).

Regarding the errors in our estimations, we found that they are due to two main reasons. First, misalignment of the angles in the moving object, e.g., our calculations in the algorithm are done assuming the tilted angles of the object are 9° , 18° , and so on, while in practice there are certain errors. Second, we assume that luminaires are single-LED sources, while in practice they have multiple LEDs (five LED sources in the case of *Shine+*). This difference changes the incidence angles, which in turn affects the estimated location. This latter point is why our errors are more pronounced at the boundaries of two beams and more accurate at the center of beams.

Finally, it is important to note that passive positioning with VLC operates in a fundamentally different manner compared to most positioning methods. Traditionally, after a signal is received, the positioning algorithm provides an estimated location that can be anywhere. In our method, the positioning algorithm only has a limited number of locations to choose from. The number of locations depends on the number of beams and tilted angles. Thus, upon receiving a signal, our method's task is to map the received signal to the most appropriate location, *without requiring a training phase*.

5.2 Positioning: Realistic Case

We now test our passive positioning in a more realistic case, consisting of less beams and an object with less tilted angels. In this scenario, we use two nodes equipped with the *Shine++* front-end. As introduced in Section 4, *Shine++* uses more powerful LEDs, which enable nodes to communicate at a distance of 5 m (the distance can be made further by increasing the light intensity of luminaires). The experimental setup in a realistic case is shown in Figure 25. In the tests, we set the height of the nodes to various levels: 1 m, 1.5 m, and 2 m. The height (range) can be increased if we add a lens to the photodiode. Meanwhile, the inter-node distance is adjusted between 2 m and 2.5 m. The light intensity measured at the floor is about 600 lux under the nodes (cf. positions $R1$ and $R5$ in Figure 27) when the height of the nodes is 1.5 m.

Dealing with floor reflection. The floor can reflect the light emitted by LEDs. When the light is modulated to send beacons, the ceiling PD can detect the transmissions of these beacons due

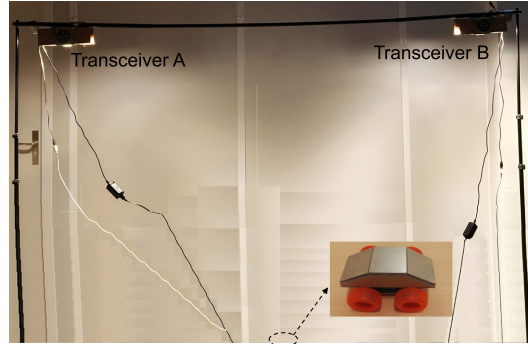


Fig. 25. Experiment setup in the realistic case.

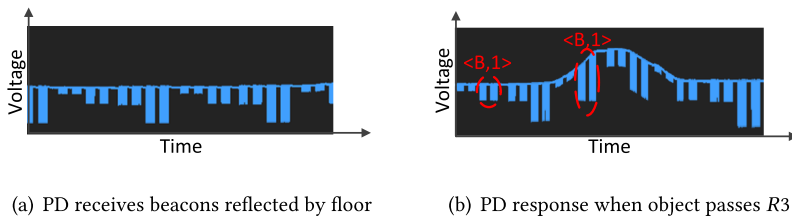


Fig. 26. Dealing with the floor reflection.

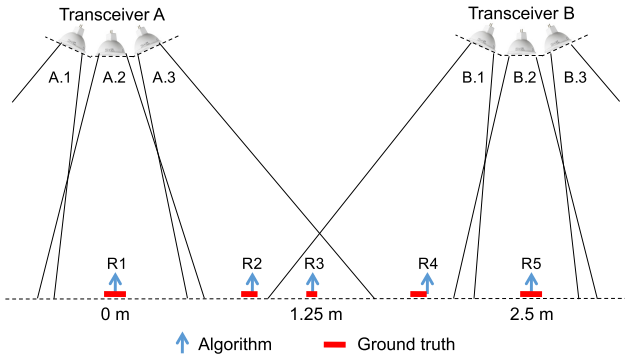


Fig. 27. Evaluation results in the realistic case (height=1.5 m, distance=2.5 m).

to the floor reflection. Figure 26(a) shows this phenomenon. When an object with a reflective surface passes under the LEDs, the PD can also detect the beacons, as illustrated in Figure 26(b). To distinguish them in order to localize the object, we design an initialization phase in which the system sends beacons and records their depths when there is no object passing by. Then, a threshold for beacon detection is calculated based on the recorded depths. When there is a beacon depth change exceeding the threshold, e.g., the beacon $\langle B, 1 \rangle$ illustrated in Figure 26(b) (the depth of other beacons remains roughly the same), our system will know which light beam has caused the above changes and then localize the object based on this information.

Results. The evaluation results are shown in Figure 27, where the height and inter-node distance are set to 1.5 m and 2.5 m, respectively. For this experiment, we use the aluminum car. All six LEDs work under the *communication+illumination* mode. First, it is important to observe that in this

Table 3. Evaluation Results in Realistic Case (Height=1 m, Inter-node Distance=2 m)

No.	R1	R2	R3	R4	R5
Reflection angle	0°	-30°	0°	25°	0°
Algorithm	0 m	0.577 m	1 m	1.534 m	2 m
Mirror	-0.02~0.02	0.63~0.66	0.99~1.01	1.48~1.51	1.98~2.02
Aluminum	-0.02~0.02	0.62~0.65	0.99~1.01	1.47~1.5	1.98~2.02

Table 4. Evaluation Results in Realistic Case (Height=1.5 m, Inter-node Distance=2.5 m)

No.	R1	R2	R3	R4	R5
Reflection angle	0°	-30°	0°	25°	0°
Algorithm	0 m	0.866 m	1.25 m	1.801 m	2.5 m
Mirror	-0.02~0.02	0.85~0.88	1.25~1.26	1.76~1.78	2.48~2.52
Aluminum	-0.02~0.02	0.85~0.88	1.25~1.26	1.77~1.79	2.48~2.52

Table 5. Evaluation Results in Realistic Case (Height=2 m, Inter-node Distance=2.5 m)

No.	R1	R2	R3	R4	R5
Reflection angle	0°	-30°	0°	25°	0°
Algorithm	0 m	1.155 m	1.25 m	1.567 m	2.5 m
Mirror	-0.02~0.02	1.15~1.17	1.25~1.27	1.5~1.52	2.48~2.52
Aluminum	-0.02~0.02	1.13~1.15	none	1.51~1.52	2.48~2.52

setup, we can only detect 5 locations, which is less than the 11 locations detected under the ideal case. This occurs because we now have less beams and less tilted angles. But all the 5 estimated locations are still accurate. Note that in Figure 27, red bars are used to represent the ground-truth positions (instead of dots as in Figure 24). This is because the surfaces are wide enough to give a continuous location range, while in Section 5.1 the mirrors are so narrow that only a “single” point is detected. Results under different inter-node distances and heights are given in Tables 3–5. These tables show the estimations of our algorithm and the ranges of the actual locations for the aluminum car and mirror car. From these results, we can observe that the maximum positioning error is around 5.3 cm and the average error is 0.97 cm. The performances with the mirror car and aluminum car are similar. The only difference is that in Table 5, the position R3 can be detected with the mirror car but not with the aluminum car (due to the lower reflective coefficient of aluminum).

5.3 Identification

We now present the evaluation on passive identification. Without loss of generality, we use the object-ID as shown in Figure 22. In the experiment, the height of the transceivers is 1.5 m and the inter-node distance is 2.5 m. The object is moved at a constant speed by a toy train motor from transceiver A to transceiver B. We only use the “standard reflector” in this test, because the “perfect reflector” is too small to carry the object-ID.

5.3.1 Results for the Scenario When LEDs Operate at Communication+illumination Mode. The signal received by the PD of transceiver A is shown in Figure 28(a). We clearly observe the high-frequency signal that contains the beam-ID, which has been successfully used for positioning in our experiment (similar to Figure 27). Furthermore, we can observe that the object-ID appears three times: In Figure 28(a), the corresponding signals are marked as G1, G2, and G3. They correspond to the three positions R1, R2, and R3 in Figure 27, where the object is located. Note that the PD

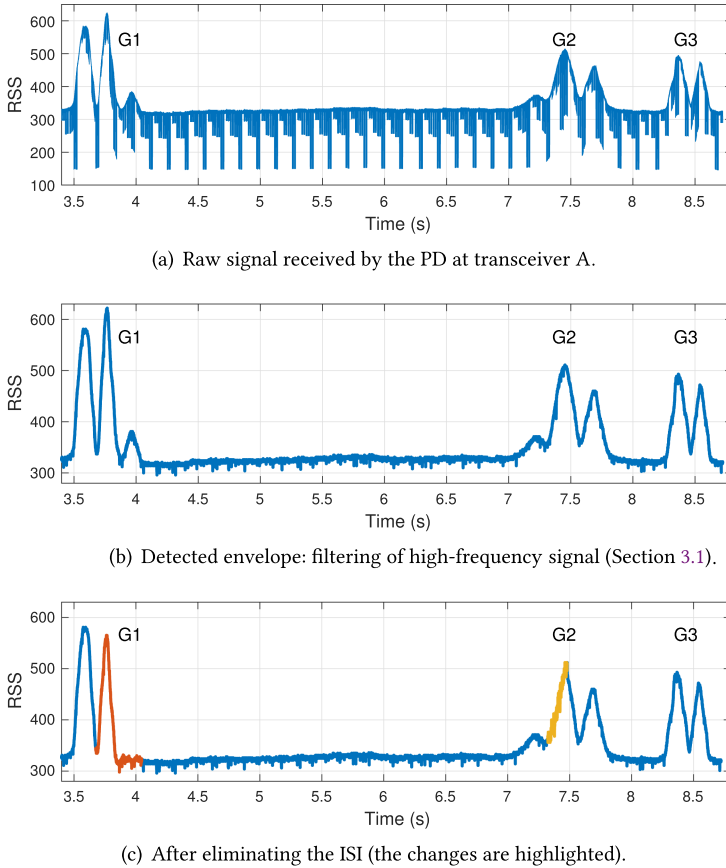


Fig. 28. Evaluation on passive identification when LEDs operate at the communication+illumination mode.

on transceiver B captures the signals of the object-ID when the object appears at the locations R_3 , R_4 , and R_5 . To decode the object-ID at these positions, we first decouple signals using the downsampling-based method presented in Section 3.1. The resulted signal is shown in Figure 28(b), which is much cleaner. In Figure 28(b), the first two groups of signals (G_1 and G_2) are affected by ISI. For G_1 , which is mapped to position R_1 , ISI takes effect at the tail. For G_2 (mapped to position R_2), ISI occurs at the beginning (τ is negative, cf. Section 3.2). For both G_1 and G_2 , we successfully used the steps presented in Section 3.2 to remove the ISI. The results are shown in Figure 28(c). For G_3 (mapped to position R_3), the object only modulates the light of one beam. Thus, ISI does not exist, and we can decode the object-ID directly.

5.3.2 Results for the Scenario When LEDs Operate at Communication Mode. When LEDs operate at the communication node, there is no ISI effect (cf. Section 3.2). However, we cannot directly obtain a clear envelope of the object-ID at the PD that can be used to decode the object-ID. Figure 29 shows the signal received by the PD of transceiver A when the object passes by the position near R_1 (cf. Figure 27). We can observe that there is no ISI effect, since no envelope of the object-ID is captured by the PD. To obtain the envelope of the object-ID, we fit the envelope of the captured signals for the same beam-ID. For instance, in Figure 29, we highlight the captured signal related to the beam $< A, 2 >$. Due to the movement of the object, the captured signal strengths are different over time. By fitting the maximal amplitudes of these captured beam-ID signals, we can

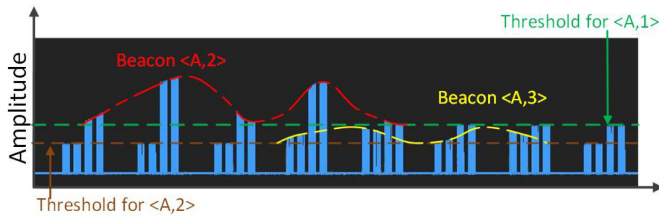


Fig. 29. Evaluation on passive identification when LEDs operate at the communication mode.

obtain the envelope of the object-ID, as shown by the red-dash line. Similarly, we can obtain the envelope of the object-ID generated due to the object's reflection of the beam $< A, 3 >$, as denoted by the yellow dashed line. After obtaining the envelope, we can decode the object-ID, as we present in Section 5.3.1. Note that if the LEDs operate at *communication+illumination* mode, the two envelopes mentioned above will overlap with each other in the time domain, starting from the beginning of the yellow dashed line.

6 RELATED WORK

Localization, both active and passive, has been investigated widely. In this section, we summarize the most relevant work.

Passive positioning with radio. M. Youssef et al. introduce the concept of Device-free Passive (DfP) positioning using Wi-Fi [Moussa and Youssef 2009; Youssef et al. 2007]. They show that changes in radio signals, caused by people, can be harnessed to localize a person. By comparing with the radio map that stores the signal strength in the area of interest [Youssef et al. 2003], the authors show that an average accuracy of 0.3 m can be achieved. Investigations in realistic environments are carried out in a follow-up work [Moussa and Youssef 2009]. Recently, researchers have also been able to track *multiple* objects passively with existing radio signals [Adib et al. 2015; Sabek et al. 2015]. High accuracies are achieved in these studies. We are motivated by these works to analyze the unique properties of visible light waves for *passive* positioning. Compared to radio waves, visible light waves behave in a more deterministic manner (less multipath) but have poorer coverage (because they cannot travel through opaque objects). Our study exposes the opportunities and limitations of exploiting the external surfaces of objects to achieve accurate positioning and identification.

Active positioning with visible light. By leveraging the built-in camera or light sensors in smartphones, researchers have exploited *active* positioning with visible light. Epsilon [Li et al. 2014] is one of such pioneer positioning systems. In Epsilon, the smartphone is enhanced with a plugged-in photosensor to detect incident lights emitted by LED lamps. Epsilon requires at least three LED lamps as anchors such that an algorithm based on trilateration can be used to calculate the smartphone's position. It can achieve accuracies of 0.4 m to 0.8 m under different indoor environments. This performance is improved by Luxapose [Kuo et al. 2014], which also adopts smartphone and LED luminaires as a receiver and transmitter, respectively. Unlike Epsilon, Luxapose leverages the angle-of-arrival of the signals in its positioning algorithm and manages to achieve a better accuracy of decimeter-level. A lightweight positioning system with visible light is proposed in Yang et al. [2015]. It leverages polarization-based modulation instead of intensity-based to reduce the processing workload in wearable devices. With these resource-constrained devices as receivers, it can achieve an accuracy of 3 m in 90% of the test cases. Complementary to existing work, LiPro [Xie et al. 2016] provides a solution for scenarios with insufficient reference points (LED bulbs). It tackles the case when there is only one reference point. By rotating the receiver (smartphone) around

three orthogonal axes, it records continuously the RSS and magnetic field, and then calculates the receiver's position by exploiting the Lambertian radiation property [Barry 1994] of LED luminaires. LiPro can achieve a median error of 0.59 m in a corridor. In D. Firoozabadi et al. [2019], the authors introduce a VLC method to tackle the underground localization problem. It exploits trilateration to calculate the target position. It can achieve an average error of 3.5 cm. Similar to these studies, we also rely on the Lambertian coverage of LED lights and the ideal attenuation properties of visible light waves to obtain positioning. But contrary to those studies, our method does not require carrying any photodetector with line-of-sight towards the luminaires—we exploit the reflective properties of external surfaces.

Passive sensing with visible light. Okuli [Zhang et al. 2015] was one of the works that inspired our PassiveVLP. Okuli uses an LED and two photodiodes to perform passive *near-field* sensing. It can track a finger's movement with a median error of 0.7 cm within an 8×8 cm pad. Okuli exploits the fact that fingers are round and good diffusers of light to build a model-driven solution, but it requires training data and a lighting system that is *specifically designed* for near-field positioning. Our system harnesses LEDs whose primary function is illumination and does not require any training to obtain only occupancy. Two other related studies are CeilingSee [Yang et al. 2017, 2018] and LocalLight [Di Lascio et al. 2016]. CeilingSee estimates occupancy by monitoring changes in light reflection caused by people in a room. CeilingSee uses general purpose luminaries, but they require a training phase to obtain only occupancy information. LocalLight deploys photosensors on floors to track people based on the shadows they cast. Compared to our work, the main advantage of these three systems is that they do not need to modify the external surfaces of the elements they track. We, however, modify the external surfaces, but obtain accurate positioning at longer ranges without requiring extra infrastructure (Okuli, LocalLight) or training phases (Okuli, CeilingSee).

Note that there is also a line of research that leverages light for secure and passive communication [Bloom et al. 2019; Wang et al. 2016; Zhang et al. 2016]. The authors in Zhang et al. [2016] design a secure system for barcode-based VLC between smartphones. In our previous work [Wang et al. 2016], we proposed a barcode-like passive VLC system with ambient light such as sunlight. Recently, we further performed a thorough analysis on how to design a barcode to transmit information on a moving object [Bloom et al. 2019]. In all those studies, the design of barcodes with visible light is key, but those systems are designed for wireless communication. In this work, PassiveVLP, we leverage visible light barcodes not only for identification but, more importantly, for localization in a passive manner.

7 LIMITATION & DISCUSSION

Many of the assumptions we make for the potential applications are realistic, such as knowing the height and geometry of luminaires. But our system also has limitations: (i) the path should not be bumpy, (ii) we can only track a few points in the paths, (iii) the system only works for 1-D scenarios, (iv) if multiple objects pass the same point simultaneously, they would cause “reflection collisions” (v) the size of the object's surface determines the maximum number of symbols that can be encoded (maximum number of IDs), and (vi) the orientation of transceivers should be stable.

Point (i) is a strong requirement—the bumpy spots in the detection area will generate outliers in our result. Our system is only resilient to few bumpy spots by eliminating outliers according to the object trace. The other five points can be improved. For point (ii), Kalman or Particle filters can be used to provide continuous location information. For point (iii), we can create annular FoVs with a single photodiode (cf. Figure 30) to provide 2D positioning (cf. Figure 31). Solving point (iv) with a single PD would be challenging, because it is hard to disaggregate colliding signals; a plausible alternative is to add more PDs with a narrower FoV to cover single lanes or tracks. Reducing the receivers' FoV would also help ameliorate point (v): A narrow FoV would allow us to use narrower

Table 6. Summary of the Most Relevant Work on Passive Localization/positioning

State of the art	Purpose	Scenario	Medium	Passive	Accuracy
[Moussa and Youssef 2009]	Localization	Indoor	Wi-Fi	Yes	0.3 m
[Adib et al. 2015]	Localization	Indoor	Radio	Yes	0.12 m
Epsilon [Li et al. 2014]	Localization	Indoor	Light	No	0.8 m
Luxapose [Kuo et al. 2014]	Localization	Indoor	Light	No	0.4 m
[Yang et al. 2015]	Localization	Indoor	Light	No	3 m
LiPro [Xie et al. 2016]	Localization	Indoor	Light	No	0.59 m
[D. Firoozabadi et al. 2019]	Localization	Underground	Light	No	0.0035 m
Okuli [Zhang et al. 2015]	Localization	Indoor	Light	Yes	0.007 m
CeilingSee [Yang et al. 2017]	Occupancy	Indoor	Light	Yes	-
Localight [Di Lascio et al. 2016]	Occupancy	Indoor	Light	Yes	-

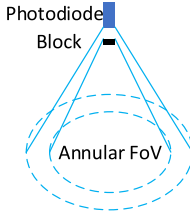


Fig. 30. Customized annular-FoV.

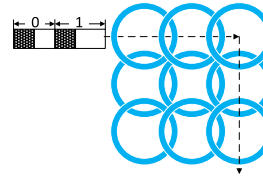


Fig. 31. 2D passive positioning.

stripes, which would increase the number of IDs that can be encoded on the object's surface. Some results can be found in our latest paper [Bloom et al. 2019]. To alleviate point (vi), we can store the light intensity caused by ground reflection after calibration. When there is no object passing by and the ground reflection does not match with the stored value well, we can then recalibrate the orientation of transceivers.

8 CONCLUSION

In this work, we took a first step to design a passive localization system, PassiveVLP, based on visible light, where objects are not required to carry photosensors. To achieve our goal, we modify the external surfaces of objects so light reflections can provide information for localization and identification. We define and analyze the elements of our proposed system and implement a testbed to benchmark its performance. Our results show that visible light can provide passive identification and localization with cm-level accuracy. Passive sensing and localization with visible light is a nascent area and, thus, there is plenty of room for future work. The results from experiments confirmed the feasibility of localizing and identifying objects with visible light. While the current implementation of our system cannot localize objects continuously, it succeeded to provide a subset of the objects' trajectory with high accuracy. We hope our work offers new insights in this up-and-coming domain.

ACKNOWLEDGMENTS

We want to thank Danielle van der Werff for proposing the idea of using annular FoVs.

REFERENCES

- Fadel Adib, Zachary Kabelac, and Dina Katabi. 2015. Multi-person localization via RF body reflections. In *Proceedings of the USENIX NSDI*.

- J. R. Barry. 1994. *Wireless Infrared Communications*. Springer.
- Rens Bloom, Marco Zuniga, Qing Wang, and Domenico Giustiniano. 2019. Tweeting with sunlight: Encoding data on mobile objects. In *Proceedings of the IEEE INFOCOM*. 1324–1332.
- G. Corbellini. 2014. Connecting networks of toys and smartphones with visible light communication. *IEEE Commun. Mag.* 52, 7 (2014).
- Elena Di Lascio, Ambuj Varshney, Thiem Voigt, and Carlos Perez-Penichet. 2016. Poster abstract: LocaLight—a battery-free passive localization system using visible light. In *Proceedings of the IPSN*.
- Ali D. Firoozabadi, Cesar Azurdia-Meza, Ismael Soto, Fabian Seguel, Nicolas Krommenacker, Daniel Iturralde, Patrick Charpentier, and David Zabala-Blanco. 2019. A novel frequency domain visible light communication (VLC) three-dimensional trilateration system for localization in underground mining. *Appl. Sci.* 9, 7 (2019).
- IEEE. 2018. *IEEE 802.11 Light Communications*. Retrieved from http://www.ieee802.org/11/Reports/tgbb_update.htm.
- L. Klaver and M. Zuniga. 2015. Shine: A step towards distributed multi-hop visible light communication. In *Proceedings of the IEEE MASS*.
- Ye-Sheng Kuo, Pat Pannuto, et al. 2014. Luxapose: Indoor positioning with mobile phones and visible light. In *Proceedings of the ACM MobiCom*.
- Jiangtao Li, Angli Liu, Guobin Shen, Liqun Li, Chao Sun, and Feng Zhao. 2015. Retro-VLC: Enabling battery-free duplex visible light communication for mobile and IoT applications. In *Proceedings of the ACM HotMobile*. 21–26.
- Liqun Li, Pan Hu, Chunyi Peng, Guobin Shen, and Feng Zhao. 2014. Epsilon: A visible light based positioning system. In *Proceedings of the USENIX NSDI*.
- Tianxing Li and Xia Zhou. 2018. Battery-free eye tracker on glasses. In *Proceedings of the ACM MobiCom*. 67–82.
- E. Mok and G. Retscher. 2007. Location determination using Wi-Fi fingerprinting versus Wi-Fi trilateration. *J. Loc. Based Serv.* 1, 2 (2007).
- M. Moussa and M. Youssef. 2009. Smart devices for smart environments: Device-free passive detection in real environments. In *Proceedings of the IEEE PerCom*.
- Philips. 2015. Philips Lighting Deploys LED-based Indoor Positioning in Carrefour Hypermarket. Retrieved from <https://goo.gl/a0tGij>.
- PureLiFi. 2012. PureLiFi. Retrieved from <http://purelifi.com>.
- I. Sabek et al. 2015. ACE: An accurate and efficient multi-entity device-free WLAN localization system. *IEEE Trans. Mob. Comput.* 14, 2 (2015).
- Qing Wang, Marco Zuniga, and Domenico Giustiniano. 2016. Passive communication with ambient light. In *Proceedings of the ACM CoNEXT*. 97–104.
- Hongjia Wu, Qing Wang, Jie Xiong, and Marco Zuniga. 2017. SmartVLC: When smart lighting meets VLC. In *Proceedings of the ACM CoNEXT*. 212–223.
- Bo Xie, Shimin Gong, and Guang Tan. 2016. LiPro: Light-based indoor positioning with rotating handheld devices. *Wirel. Netw.* 24, 1 (2016).
- Xieyang Xu, Yang Shen, Junrui Yang, Chenren Xu, Guobin Shen, Guojun Chen, and Yunzhe Ni. 2017. PassiveVLC: Enabling practical visible light backscatter communication for battery-free IoT applications. In *Proceedings of the ACM MobiCom*. 180–192.
- Yanbing Yang, Jie Hao, Jun Luo, and Sinno Jialin Pan. 2017. CeilingSee: Device-free occupancy inference through lighting infrastructure based LED sensing. In *Proceedings of the IEEE PerCom*.
- Yanbing Yang, Jun Luo, Jie Hao, and Sinno Jialin Pan. 2018. Counting via LED sensing: Inferring occupancy using lighting infrastructure. *Elsevier Perv. Mob. Comput.* 45, 1 (2018), 35–54.
- Zhice Yang et al. 2015. Wearables can afford: Light-weight indoor positioning with visible light. In *Proceedings of the ACM MobiSys*.
- M. Youssef, A. Agrawala, and A. Shankar. 2003. WLAN location determination via clustering and probability distributions. In *Proceedings of the IEEE PerCom*.
- Moustafa Youssef, Matthew Mah, and Ashok Agrawala. 2007. Challenges: Device-free passive localization for wireless environments. In *Proceedings of the ACM MobiCom*.
- B. Zhang, K. Ren, G. Xing, X. Fu, and C. Wang. 2016. SBVLC: Secure barcode-based visible light communication for smartphones. *IEEE Trans. Mob. Comput.* 15, 2 (2016), 432–446.
- Chi Zhang, Josh Tabor, Jiali Zhang, and Xinyu Zhang. 2015. Extending mobile interaction through near-field visible light sensing. In *Proceedings of the ACM MobiCom*.
- Chi Zhang and Xinyu Zhang. 2017. Pulsar: Towards ubiquitous visible light localization. In *Proceedings of the ACM MobiCom*. 208–221.

Received December 2018; revised July 2019; accepted July 2019